

Communication

Open Access



Intense pulsed light-induced selective conversion of printed silicon nanoparticles into graphene embedding silicon carbide on plastic for the next generation flexible lithium-ion batteries

Jawad Reslan¹, Omar Kassem^{1,2}, Vincent Barnier², Sergio Sao-joao², Florence Vacandio³, Mohamed Saadaoui¹ , Thierry Djenizian^{1,4,*}

¹Department of Flexible Electronics, Mines Saint-Etienne, Center of Microelectronics in Provence, Gardanne F - 13541, France.

²Mines Saint-Etienne, Université de Lyon, CNRS, UMR 5307 LGF, Centre SPIN, Saint-Etienne F-42023, France.

³Aix Marseille Université, CNRS, MADIREL, UMR 7246, Marseille 13397, France.

⁴Al-Farabi Kazakh National University, Center of Physical-Chemical Methods of Research and Analysis, Almaty 050040, Kazakhstan.

*Correspondence to: Prof. Thierry Djenizian, Department of Flexible Electronics, Mines Saint-Etienne, Center of Microelectronics in Provence, 880 Rte de Mimet, Gardanne F - 13541, France. E-mail: thierry.djenizian@emse.fr

How to cite this article: Reslan, J.; Kassem, O.; Barnier, V.; Sao-joao, S.; Vacandio, F.; Saadaoui, M.; Djenizian, T. Intense pulsed light-induced selective conversion of printed silicon nanoparticles into graphene embedding silicon carbide on plastic for the next generation flexible lithium-ion batteries. *Energy Mater.* **2025**, *5*, 500137. <https://dx.doi.org/10.20517/energymater.2025.12>

Received: 17 Jan 2025 **First Decision:** 3 Mar 2025 **Revised:** 31 Mar 2025 **Accepted:** 22 May 2025 **Published:** 24 Jul 2025

Academic Editor: Ho Seok Park **Copy Editor:** Ping Zhang **Production Editor:** Ping Zhang

Abstract

Silicon is a promising anode material for next-generation lithium-ion batteries (LIBs) due to its high theoretical capacity. However, its practical use is hindered by significant volume expansion during charge cycles, which causes poor cycling stability. Intense pulsed light technology offers a solution through rapid, selective heating, enabling nanoscale transformations without damaging substrates. Here, a scalable approach for creating silicon patterns on polymer foils and converting them into nanoscale composite layers under ambient conditions is presented. The use of inkjet printing in conjunction with intense Pulsed Light treatment is demonstrated to generate localized temperatures in excess of 1,940 °C within milliseconds, whilst maintaining the integrity of the polymer substrate. This rapid heating method induces local carbonization of the polymer, thereby converting the Si nanoparticles into a new silicon carbide (SiC) embedded in a few-layer graphene composite electrode. The resulting heterostructure anode exhibits excellent electrochemical performance, improved cycling stability, and enhanced rate capability, positioning it as a promising binder-free silicon anode for next-generation lithium-ion batteries.

Keywords: Silicon nanoparticles, silicon carbide, multi-layer graphene, inkjet printing, intense pulsed light, lithium-ion batteries



© The Author(s) 2025. **Open Access** This article is licensed under a Creative Commons Attribution 4.0 International License (<https://creativecommons.org/licenses/by/4.0/>), which permits unrestricted use, sharing, adaptation, distribution and reproduction in any medium or format, for any purpose, even commercially, as long as you give appropriate credit to the original author(s) and the source, provide a link to the Creative Commons license, and indicate if changes were made.



INTRODUCTION

The growing demand for high-energy-density flexible lithium-ion batteries (LIBs) is driven by increasing demand for autonomous and flexible electronic market such as wearable and implantable medical devices, autonomous sensors, smart garments and roll-up mobile phones. These requirements pose significant challenges toward the development of high-performance flexible LIBs that are capable of withstanding mechanical deformation, including bending, folding, and stretching.

The development of flexible electrodes is one of the relevant keys to achieving high-performance and flexible LIBs. Freestanding composite electrodes are usually preferred and they are prepared by mixing either carbon-based materials such as carbon nanotubes, nanofibers and graphene foams or MXene with nanoscaled active materials such as Fe_2O_3 , $\text{Fe}_2\text{O}_3/\text{MoS}_2$, Si, Ge, SnS_2 , *etc.*^[1-6]. Such electrodes exhibiting high mechanical flexibility can further enhance anode capacity by avoiding the use of a metal current collector.

Silicon is regarded as a promising anode material due to its theoretical gravimetric capacity ($3,580 \text{ mA h g}^{-1}$ at room temperature), over ten times greater than that of conventional graphite (372 mA h g^{-1})^[7-9], low delithiation potential ($< 0.5 \text{ V vs. Li}^+/\text{Li}$) and abundance. In order to circumvent the large-volume expansion that occurs during the lithiation phase and to improve electrical conductivity, Si is frequently utilized at the nanoscale level and combined synergistically with carbon-based materials^[10]. Zhang *et al.*^[11] developed a freestanding Si@C bonded to MXene Electrode exhibiting superior mechanical flexibility and stable performances with a capacity of $1,040 \text{ mA h g}^{-1}$ after 150 cycles at 420 mA g^{-1} . Another approach consists of mixing graphene/Si composite in a polymer matrix of poly(1-pyrenebutyl methacrylate) (PBuPy) and poly(1-pyrenebutyl methacrylate-co-methacrylic acid) (PBuPyMAA). The combination of pyrene and butyl in interaction with the graphene enhances the mechanical and electrical integrity of the anode, achieving a volumetric capacity of over $1,700 \text{ Ah L}^{-1}$ at 333 mA g^{-1} ^[12].

Recent studies show that the combination of graphene with silicon carbide (SiC) improves both electronic conductivity and lithium-ion transport in LIBs. When graphene is combined with SiC, it stabilizes the electrode, buffers the mechanical stress during silicon expansion, and enhances structural integrity. These effects lead to better capacity of $1,820 \text{ mAh g}^{-1}$ over 200 cycles at a 1C rate, making graphene a valuable addition to LIB anodes^[13]. Moreover, The SiC layer has been demonstrated to enhance the interfacial adhesion between silicon and graphene through the covalent phase and impedes the formation of Li_2SiF_6 aggregates during cycling, thus lowering Li-ion consumption and improving mechanical stability thanks to the high strength and toughness of SiC^[13]. However, synthesizing nanostructured SiC with controlled morphology embedded in graphene is challenging due to the high processing temperatures required (above $1,200^\circ\text{C}$). Achieving this process on flexible substrates such as polymer substrates is advantageous and challenging at the same time due to the limited operating temperature window of polymer substrates, as it enables the development of lightweight and adaptable devices while eliminating the need for the current collector, offering improved flexibility and reduced material constraints.

Herein, we demonstrate the effectiveness of intense pulsed light (IPL) in producing graphene/silicon carbide nano-composite electrodes on a flexible polyimide foil at ambient conditions. Inkjet-printed silicon nanoparticles on polyimide submitted to intense white light were instantaneously converted into SiC nanocrystals embedded in graphene thanks to the strong photothermal effect. The heat absorbed by the silicon nanoparticles (around $1,900^\circ\text{C}$) locally carbonizes the interfacial polyimide that acts as a carbon source, without degrading the overall mechanical flexibility of the polyimide. The resulting graphene/SiC

heterostructure anode shows excellent electrochemical performance, including improved cycling stability and rate capability. By addressing the volume expansion and conductivity issues inherent in Si anodes, this scalable, current-collector and binder-free approach offers a promising solution for high-performance flexible next-generation micro-LIBs.

EXPERIMENTAL

Materials

Si nanoparticles ink was purchased from Meliorum Technologies (Rochester, USA), with nanoparticles of 30 nm diameter and a purity of 99.9% (metals basis). These nanoparticles are encapsulated in an organic material that protects the surface of the Si from oxidation in the air and ensures that they are evenly dispersed within the ink and during the printing process. The composition of the protective layer is a trade secret.

Inkjet printing of Si ink

The ink composition consists of 1 wt% Si nanoparticles dispersed in ethylene glycol, giving it a surface tension of approximately 48 mN/m. To achieve a well-homogenized pattern of Si nanoparticles, optimum printing parameters were carefully established. The high surface tension of the ink compared to the low surface energy of the upilex substrate (~36 mN/m) prevents the spreading of the ink. To overcome this, the substrate was O₂ plasma treated to increase its surface energy, allowing the ink to spread evenly across the patterned area. Commercial Dimatix DMP-2800 (Fujifilm Dimatix, Inc., USA) was used for inkjet printing. Furthermore, the substrate holder of the printer was heated to 45 °C to trigger solvents evaporation on the substrate and to confine printed line resolution. The drop spacing was adjusted to a 20° angle. The printer default waveform was used to ensure that the ink droplets maintained a spherical shape during ejection. These carefully tuned parameters resulted in a uniform and homogeneous Si nanoparticle pattern. Due to the low weight percentage of Si in the ink, 50 consecutive layers had to be printed to achieve a 3 µm thick Si film. A dry-on-wet approach was used, where the printed layers were partially dried after every ten layers before continuing deposition. This method allows the underlying layers to retain some residual solvent, maintaining surface wettability and promoting better adhesion between successive layers. At the same time, the controlled drying prevents excessive accumulation of liquid, which could lead to uncontrolled spreading or pattern distortion due to the well-known coffee-ring effect. This approach not only facilitated uniform layer build-up but also ensured that the ink remained confined to the intended pattern, preventing unwanted spreading.

Intense pulsed light of printed Si

Intense pulsed light was performed on the PulseForge 3200 - X1 (PulseForge - USA). The system is equipped with a set of two xenon lamps that emit an intense and broad spectrum of light. The radiant energy of the emitted light was recorded using a BX-100 bolometer. All experiments were performed in the air under atmospheric conditions.

Characterization and electrochemical tests

An ultraviolet-visible (UV-VIS) spectrophotometer equipped with a sphere was used to determine the optical absorbance “A” of printed and dried Si thin film from the measured transmittance “T” and total reflectance “R” ($A = 100\% - T - R$). High-resolution transmission electron microscopy (HRTEM) imaging was carried out at 200 keV using a Thermo Fisher Titan microscope equipped with a field emission gun and a spherical aberration (Cs) corrector. Prior to transmission electron microscopy (TEM) imaging, the samples were prepared into ultra-thin membranes using Leica UC6/FC6 ultramicrotome. Raman spectra were acquired before and after IPL annealing using a 514 nm excitation wavelength. The microstructures of the printed Si films were studied using scanning electron microscopy (SEM) (JEOL JSM-7800F). The electrical

resistivities were measured in a 4-point probe configuration. The printed Si film was assembled in a Swagelok cell with a 10 mm disk of lithium metal foil as the counter electrode and a 10 mm disk of Whatman microfiber glass as the separator in an argon-filled glove box. The organic liquid electrolyte used consisted of 1M LiPF₆ salt dissolved in a 1:1 volume ratio of ethylene carbonate and diethyl carbonate (EC:DEC). Galvanostatic discharge/charge cycling of half-cell was performed within a voltage range of 0.05–3 V. Cyclic voltammetry (CV) was conducted at 0.05 mV s⁻¹ between 0.05–3 V. Electrochemical Measurements were conducted using a VMP3 potentiostat-galvanostat (BioLogic) and capacities were determined relative to the weight of active material.

RESULTS AND DISCUSSION

The inkjet-printed Si pattern on upilex exhibits broadband light absorption across the visible range, which matches the emission spectrum of xenon lamp [Figure 1A]. This optical absorptance capability ensures efficient heat generation on the Si nanoparticles through the photothermal effect. IPL annealing was then performed to evaporate residual ethylene glycol, to decapsulate the Si nanoparticles from the organic layer and to trigger the sintering process.

The pulse profile was optimized to ensure volumetric heat in the Si thin-film, while keeping the backside temperature below the polymer thermal threshold (below 500 °C). Due to the limited lifespan of the xenon lamps, the number of consecutive pulses had to be restricted. As a result, the pulses were delivered in multiple cycles and repeated three times at 4 Hz [Figure 1B and C].

SimPulse software was used to calculate the temperature at the surface of Si thin-film using measured optical absorptance and thermal properties of silicon and polyimide foil given in Supplementary Table 1. Figure 1C shows the simulated temperature evolution at the surface of the printed Si thin film under a sequence of eight pulses, repeated three times. As expected, the Si thin film quickly heated up rapidly after each pulse due to the combined photothermal effect and heat accumulation between consecutive pulses. In the first cycle, the underside of the polyimide substrate remained at a low temperature and then gradually reached up to 490 °C during the following cooling phase. The cycling frequency of 4 Hz was optimized to allow sufficient time for the Si surface to cool to a safe level before each new cycle, preventing the delamination of the Si thin film and the degradation of the polyimide substrate. The cooling interval was fine-tuned to keep the underside of the polymer substrate below its maximum operating temperature to avoid damage.

The simulated temperatures are higher than the melting point of bulk silicon (1,415 °C), which is lower for Si nanoparticles due to their small size. These high temperatures are sufficient to decapsulate the Si nanoparticles. Under these conditions, SiC and graphene are formed on the plastic. This is due to the solubility of carbon in silicon (see Figure 2A)^[14] in conjunction with the local graphitization of the upilex that acts as a carbon source^[15]. Finally, we can also expect the chemical reduction of SiO₂ to Si at the surface of Si nanoparticles, thanks to the presence of C, according to



In consideration of these results and the simulated temperature of IPL-treated Si thin film, we can further conclude that Si nanoparticles film will undergo interfacial interaction with carbon coming from the surface of upilex, thereby forming a new composite material. Subsequently, Raman spectroscopy was then performed on the IPL-treated Si patterns at a wavelength of 532 nm. The as-printed and dried Si pattern (90 °C for 6 h to remove ethylene glycol and to avoid excessive coffee ring) shows a characteristic peak of

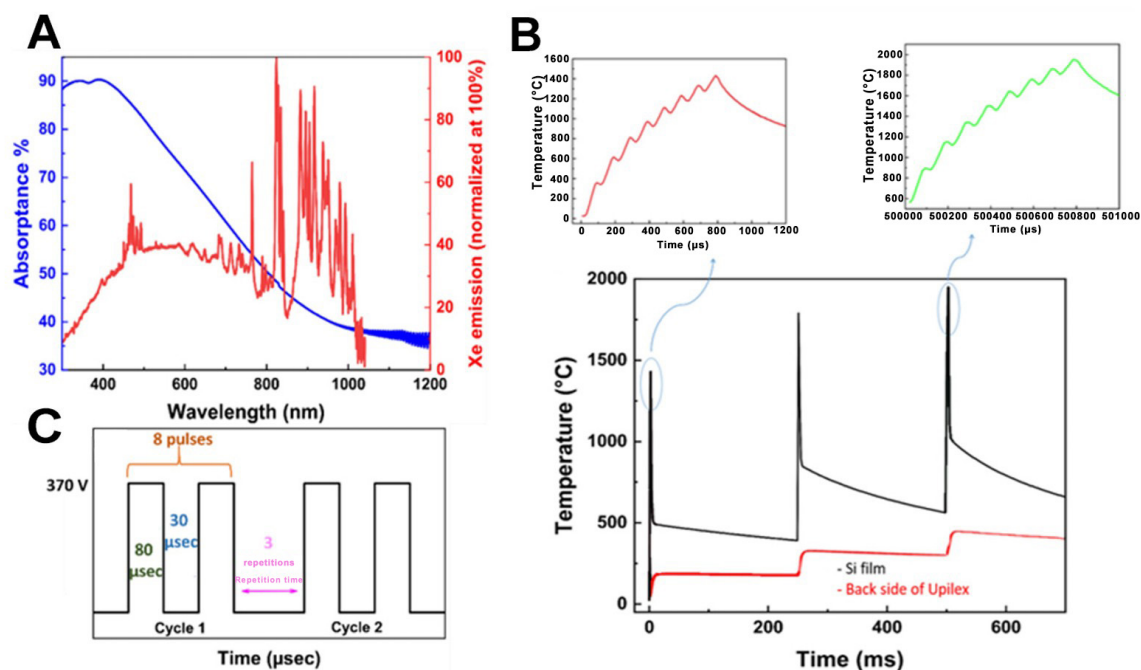


Figure 1. (A) Optical absorbance vs. wavelength; (B) Schematic representation of the IPL parameters; (C) Temperature evolution during optimal IPL conditions (8 pulses in each cycle). IPL: Intense pulsed light.

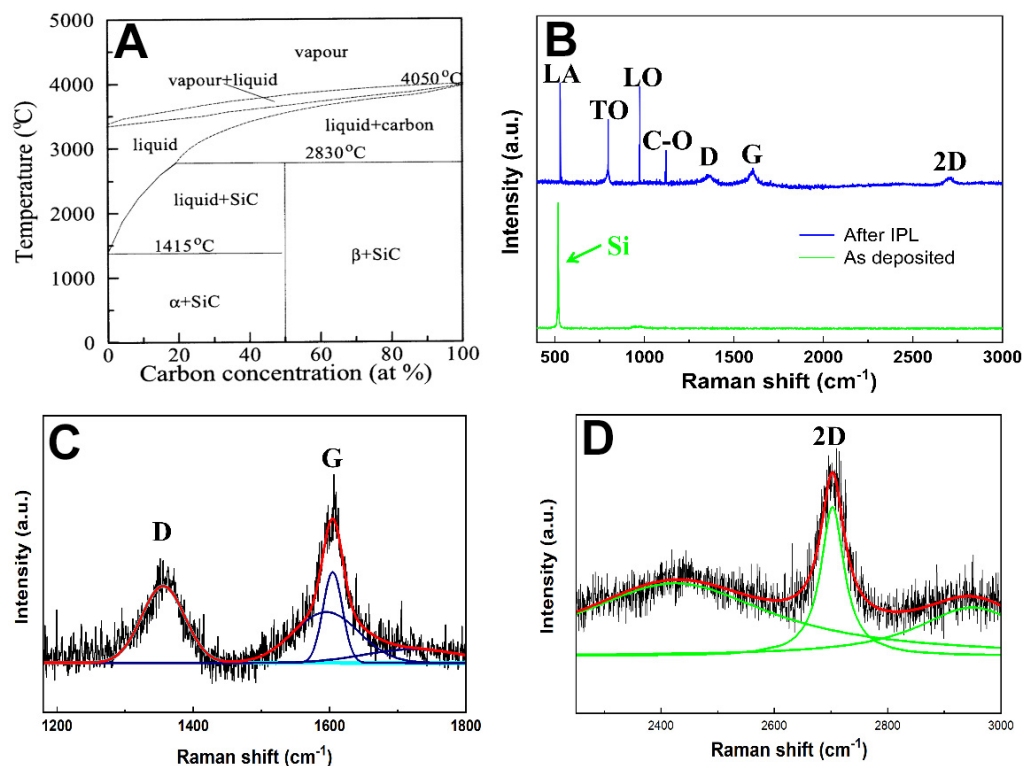


Figure 2. (A) Equilibrium phase diagram of the carbon-silicon system^[14], Copyright © 1969, Springer; (B) Raman spectrum acquired from the graphene embedded 3C-SiC nanocrystal; (C) fit of D and G peaks (three Gaussians) and (D) fit of 2D peak (one Lorentzian).

silicon at 520 cm^{-1} [Figure 2B]. Following IPL treatment, distinct and sharp peaks corresponding to SiC vibrational modes were identified [Figure 2B], including longitudinal acoustic (LA), transverse optical (TO), and longitudinal optical (LO) modes at 529.3 , 798.4 , and 973.8 cm^{-1} , respectively^[16-18]. Moreover, a peak at $1,122\text{ cm}^{-1}$ corresponds to the phonon mode of C-O [Figure 2B]^[16]. The position of these peaks is indicative of the formation of the silicon carbide 3C-SiC polytype.

Furthermore, Raman analysis detected the characteristic G, and 2D bands at $1,604$ and $2,702\text{ cm}^{-1}$, respectively [Figure 2C and D], thus confirming the formation of graphene within SiC. The fitting of the 2D peak with a single Lorentzian confirms the presence of multi-layer graphene^[19] [Figure 2D], which is in accordance with the TEM picture shown in Figure 3.

The signature of the D peak at $1,355\text{ cm}^{-1}$ is indicative of structural defects within graphene [Figure 2B], with the I_D/I_G ratio measured at 0.84 . The fit of the G peak shows three components. The peak at $1,604\text{ cm}^{-1}$ indicates the formation of graphene. The other two peaks, at $1,594\text{ cm}^{-1}$ and $1,726\text{ cm}^{-1}$, are attributable to the carbon present within the SiC structure [Figure 2C].

The polycrystalline nature of the annealed Si film was confirmed by the selective area electron diffraction (SAED) pattern [Figure 3A]. The diffraction rings observed in the SAED pattern were indexed to the (111) and (220) crystal planes of 3C-SiC, providing further validation of the formation of pure 3C-SiC in the annealed electrodes. HRTEM of the cross-section of the annealed Si film [Figure 3B] further supported these findings. The HRTEM lattice image revealed the formation of 3C-SiC, characterized by a d-spacing of 0.25 nm , confined within multi-layer graphene, characterized by a d-spacing of 0.335 nm .

Supplementary Figure 1A and B shows SEM images of the printed and dried Si electrodes before IPL treatment. The as-deposited film is homogeneous with high packing density of the Si nanoparticle. The average Si particle mean diameter is approximately 30 nm . Supplementary Figure 1C and D shows SEM images of the electrode following IPL treatment and exhibiting significant alterations. The images obtained reveal the presence of SiC particles embedded within a carbonaceous matrix, which is likely to be graphene. It is evident that the Si nanoparticles have melted and reacted with carbon during IPL, resulting in the formation of larger SiC particles with an average mean diameter of 250 nm . Surrounding these larger SiC particles are smaller carbon-based domains ($\sim 10\text{ nm}$) which are observed to be smaller than the original mean diameter of Si nanoparticle size and may correspond to graphene structures. Furthermore, indications of carbonization and graphitization of the upilex substrate are discernible in the proximity of the IPL treated Si pattern. These analyses confirm the conversion of Si nanoparticles patterns into 3C-SiC, which is embedded into multi-layer graphene on plastic at ambient conditions. At high temperatures, upilex carbonizes locally at the interface and acts as a carbon source that reacts with Si nanoparticles to form SiC and graphene. These results are in accordance with literature that reported that the carbon solubility into silicon is limited by the formation of 3C-SiC^[20]. According to Si/C phase diagram [Figure 2B], we can expect the formation of 3C-SiC for carbon concentration above $50\text{ at.}\%$ at temperature of $1,940^\circ\text{C}$.

To our knowledge, this is the first demonstration of SiC embedded in graphene on a flexible plastic substrate at ambient conditions [Supplementary Figure 2]. Most proposed techniques rely on heating the SiC substrate above a critical temperature under ultra-high vacuum condition which triggers the sublimation of Si atoms and forms a high-quality graphene film over SiC^[21]. Laser and e-beam are two methods that were reported as selective methods to induce graphene on SiC^[22].

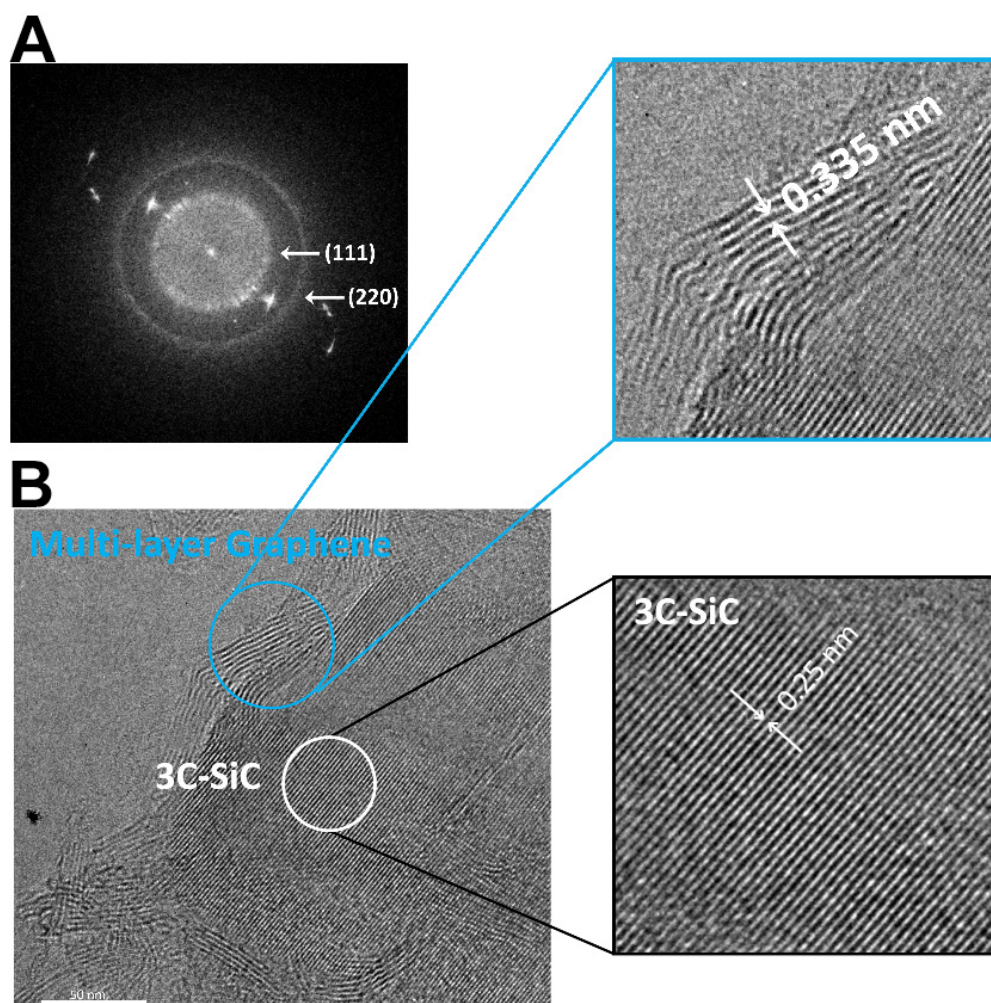


Figure 3. (A) A typical SAED pattern recorded from IPL treated Si; (B) HRTEM image of graphene embedded 3C-SiC. SAED: Selective area electron diffraction; IPL: intense pulsed light; HRTEM: high-resolution transmission electron microscopy.

First, the electrochemical performance of inkjet-printed and dried Si nanoparticles was evaluated [Supplementary Figure 3]. The high initial discharge capacity is primarily due to the formation of solid electrolyte interface (SEI). However, a sharp decline in capacity becomes evident from the second cycle onwards. This poor performance may be attributed to the volume expansion of the Si nanoparticles or to the presence of an encapsulating layer surrounding the Si nanoparticles. This organic layer may hinder lithium insertion and significantly limit the electrochemical activity. Whilst this encapsulation layer improves nanoparticle dispersion and printability, it ultimately impedes the lithiation/delithiation process. Subsequently, we evaluated the electrochemical performance of the SiC/graphene electrodes were fabricated on upilex by irradiating the Si nanoparticle ink with an emitted energy of of 9.57 J/cm². Figure 4A presents the CV curves for the initial five cycles. The scan range is set from 2.5 V to 0.25 V, with a scan speed of 0.05 mV s⁻¹. During the initial discharge process, reduction peaks are observed around 1.28, 0.37, and 0.2 V (vs. Li/Li⁺). The broad feature observed at 1.28 V is attributed to interfacial reaction between the electrode surface and the electrolyte. The peak at 0.37 V is indicative of the lithiation of silicon, resulting in the formation of lithium-silicon alloys ($x\text{Si} + \text{Li} \rightarrow \text{Li}_x\text{Si}$)^[23]. This suggests the presence of residual Si nanoparticles after IPL treatment, which are not fully converted into SiC, while the signal near 0.2 V is associated with lithium insertion into conductive carbon domains^[24–26]. No characteristic peaks were

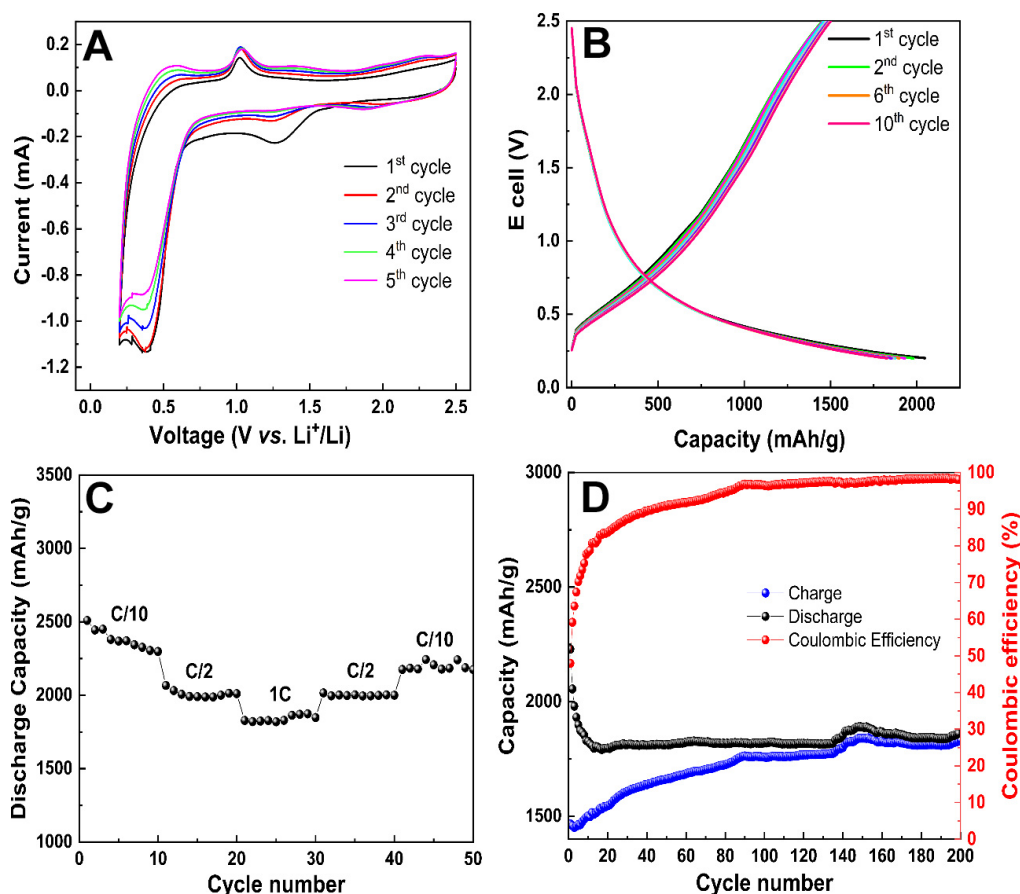


Figure 4. Electrochemical performance of SiC/graphene anode for LIB. (A) Cyclic voltammetry of the 1st to 5th cycles in a voltage range of 0.25–2.5 V at a sweep rate of 0.05 mV s⁻¹; (B) Galvanostatic charge/discharge at 1C; (C) Multi-C-rate performance of SiC/graphene; (D) long term cycling performance at 1C. LIB: Lithium-ion batteries.

observed for SiC, which is consistent with literature reports^[27,28]. Concurrently, two substantial oxidation peaks are discerned at 0.52 V and 1 V, corresponding to the delithiation of the lithium-silicon alloy ($\text{Si}_x\text{Li} \rightarrow x\text{Si} + \text{Li}$) and lithium extraction from carbon, respectively, in the anodic scan curve^[29]. Subsequent cycles demonstrate a high degree of similarity with the initial CV, exhibiting nearly identical CV curves.

As shown in Figure 4B, the galvanostatic cycling performance of the SiC/graphene electrodes at a current density of 1C (1 A/g) reveals a high initial discharge capacity of 2,050 mAh g⁻¹ during the first discharge cycle. However, following the initial cycle, the charge and discharge curves nearly overlap, indicating the superior cycling stability of the SiC/graphene composite electrodes.

The SiC electrode demonstrated significant cycling performances, as shown in Figure 4C. As the current density increased from 100 to 500 and 1,000 mA/g, the discharge capacity remained high, with values of 2,509, 2,066, and 1,828 mAh g⁻¹, respectively. To the 50th cycle, the current density was reduced to 100 mA g⁻¹, resulting in a partial recovery of the capacity to 2,175 mAh g⁻¹, thereby regaining approximately 86% of its initial specific capacity. This recovery further underscores the resilience and stability of the SiC electrode under varying conditions. Moreover, the long-term cycling performance of SiC at high rate of 1 A g⁻¹ was evaluated [Figure 4D]. After an initial discharge capacity loss and concurrent increase in charge capacity, the SiC electrode gradually stabilized, maintaining a reversible capacity of approximately

1,856 mAh g⁻¹ after 200 cycles. The progressive convergence between discharge and charge capacities led to an increase in coulombic efficiency, which stabilized around 99% as the capacity reached nearly a steady state, emphasizing the superior lithium storage capacity and cycling stability of the SiC electrode. A detailed comparison of the electrochemical performance of various approaches reported in the literature is presented in [Supplementary Table 2](#), demonstrating that our approach outperforms all previously reported methods in terms of capacity and cycling stability.

CONCLUSION

In this study, we successfully developed a novel approach for fabricating high-performance, binder-free and current collector-free SiC/graphene electrodes for next-generation LIBs. By combining inkjet printing with IPL irradiation, we were able to create uniform Si patterns on polyimide foils and convert them into a graphene-embedded SiC nanocrystal. This innovative method not only addresses the inherent challenges of Si anodes, such as volume expansion and poor electrical conductivity, but also enhances the structural stability and electrochemical performance of the anode material.

The SiC/graphene electrodes demonstrated good cycling stability, with a high initial capacity of 2,536 mAh g⁻¹ and a reversible capacity of 1,820 mAh g⁻¹ over 200 cycles at a 1C rate. Moreover, the electrodes exhibited remarkable performance at higher current densities, maintaining a high discharge capacity even at high c-rates, and showed significant capacity recovery (77%) when cycling conditions were adjusted. These results highlight the potential of SiC/graphene as a promising anode material for high-energy-density LIBs with a long cycle life.

The scalable fabrication process outlined in this work provides a viable pathway for the development of advanced, cost-effective, and durable anode materials for portable electronics, electric vehicles, and renewable energy storage systems, where further studies of lithiation/delithiation mechanism and electrochemical performances of SiC/graphene under bending test will be done in the near future making it a promising candidate for next-generation flexible LIBs technologies.

DECLARATIONS

Authors' contributions

Wrote and reviewed the manuscript: Reslan, J.; Saadaoui, M.; Djenizian, T.

Made substantial contributions to conception and design of the study and performed data analysis and interpretation: Reslan, J.; Kassem, O.; Barnier, V.; Sao-Joao, S.; Saadaoui, M.

Performed data acquisition and provided administrative, technical, and material support: Reslan, J.; Kassem, O.; Barnier, V.; Saadaoui, M.; Vacandio, F.

Availability of data and materials

The data that support the findings of this study are available from the corresponding author upon reasonable request.

Financial support and sponsorship

This work has been supported by the Région Sud and partially funded by the research project «HIPERSLIM» ANR21CE050009.

Conflicts of interest

All authors declared that there are no conflicts of interest.

Ethical approval and consent to participate

Not applicable.

Consent for publication

Not applicable.

Copyright

© The Author(s) 2025.

REFERENCES

- Karam, Z.; Susantyoko, R. A.; Alhammadi, A.; Mustafa, I.; Wu, C.; Almheiri, S. Development of surface-engineered tape-casting method for fabricating freestanding carbon nanotube sheets containing Fe₂O₃ nanoparticles for flexible batteries. *Adv. Eng. Mater.* **2018**, *20*, 1701019. DOI
- Huang, X.; Cai, X.; Xu, D.; et al. Hierarchical Fe₂O₃@CNF fabric decorated with MoS₂ nanosheets as a robust anode for flexible lithium-ion batteries exhibiting ultrahigh areal capacity. *J. Mater. Chem. A* **2018**, *6*, 16890-9. DOI
- Mo, R.; Rooney, D.; Sun, K.; Yang, H. Y. 3D nitrogen-doped graphene foam with encapsulated germanium/nitrogen-doped graphene yolk-shell nanoarchitecture for high-performance flexible Li-ion battery. *Nat. Commun.* **2017**, *8*, 13949. DOI PubMed PMC
- Wang, M.; Huang, Y.; Zhu, Y.; Wu, X.; Zhang, N.; Zhang, H. Binder-free flower-like SnS₂ nanoplates decorated on the graphene as a flexible anode for high-performance lithium-ion batteries. *J. Alloys. Compd.* **2019**, *774*, 601-9. DOI
- Kuang, Y.; Chen, C.; Pastel, G.; et al. Conductive cellulose nanofiber enabled thick electrode for compact and flexible energy storage devices. *Adv. Energy. Mater.* **2018**, *8*, 1802398. DOI
- Luo, S.; Wang, K.; Wang, J.; Jiang, K.; Li, Q.; Fan, S. Binder-free LiCoO₂/carbon nanotube cathodes for high-performance lithium ion batteries. *Adv. Mater.* **2012**, *24*, 2294-8. DOI
- Huang, J.; Li, J.; Ye, L.; et al. Synthesis of Si/C composites by silicon waste recycling and carbon coating for high-capacity lithium-ion storage. *Nanomaterials* **2023**, *13*, 2142. DOI PubMed PMC
- Szczec, J. R.; Jin, S. Nanostructured silicon for high capacity lithium battery anodes. *Energy. Environ. Sci.* **2011**, *4*, 56-72. DOI
- Zhao, L.; Ding, B.; Qin, X. Y.; et al. Revisiting the roles of natural graphite in ongoing lithium-ion batteries. *Adv. Mater.* **2022**, *34*, 2106704. DOI
- Yang, Y.; Yuan, W.; Kang, W.; et al. Silicon-nanoparticle-based composites for advanced lithium-ion battery anodes. *Nanoscale* **2020**, *12*, 7461-84. DOI
- Zhang, P.; Zhu, Q.; Guan, Z.; Zhao, Q.; Sun, N.; Xu, B. A flexible Si@C electrode with excellent stability employing an MXene as a multifunctional binder for lithium-ion batteries. *ChemSusChem* **2020**, *13*, 1621-8. DOI
- Zheng, T.; Jia, Z.; Lin, N.; et al. Molecular spring enabled high-performance anode for lithium ion batteries. *Polymers* **2017**, *9*, 657. DOI PubMed PMC
- Yu, C.; Chen, X.; Xiao, Z.; et al. Silicon carbide as a protective layer to stabilize Si-based anodes by inhibiting chemical reactions. *Nano. Lett.* **2019**, *19*, 5124-32. DOI
- Olesinski, R. W.; Abbaschian, G. J. The C-Si (carbon-silicon) system. *Bull. Alloy. Phase. Diagr.* **1984**, *5*, 486-9. DOI
- Durand, F.; Duby, J. C. Carbon solubility in solid and liquid silicon-a review with reference to eutectic equilibrium. *JPE.* **1999**, *20*, 61-3. DOI
- Jeong, J.; Chung, G.; Nishino, S. Raman scattering investigation of polycrystalline 3C-SiC film deposited on SiO₂ by using APCVD with hexamethyldisilane. *J. Korean. Phy. Soc.* **2008**, *52*, 43-7. DOI
- Raju, M.; Sen, S.; Sarkar, D.; Jacob, C. Synthesis of 3C-silicon carbide 1D structures by carbothermal reduction process. *J. Alloys. Compd.* **2021**, *857*, 158243. DOI
- Gouider Trabelsi A, V Kusmartsev F, Kusmartseva A, H Alkallas F, AlFaify S, Shkir M. Raman spectroscopy imaging of exceptional electronic properties in epitaxial graphene grown on SiC. *Nanomaterials* **2020**, *10*, 2234. DOI PubMed PMC
- Negishi, R.; Yamamoto, K.; Kitakawa, H.; et al. Synthesis of very narrow multilayer graphene nanoribbon with turbostratic stacking. *Appl. Phys. Lett.* **2017**, *110*, 201901. DOI
- Bean, A.; Newman, R. The solubility of carbon in pulled silicon crystals. *J. Phys. Chem. Solids.* **1971**, *32*, 1211-9. DOI
- Zebardastan, N.; Bradford, J.; Lipton-Duffin, J.; et al. High quality epitaxial graphene on 4H-SiC by face-to-face growth in ultra-high vacuum. *Nanotechnology* **2022**, *34*, 105601. DOI
- Lu, L.; Zhang, D.; Xie, Y.; He, H.; Wang, W. Laser induced graphene/silicon carbide: core-shell structure, multifield coupling effects, and pressure sensor applications. *Adv. Mater. Technol.* **2022**, *7*, 2200441. DOI
- Shi, H.; Wang, J.; Wang, C.; et al. Design of supported-coated structure silicon/carbon composites using industrial waste micrometer-sized silicon for an advanced lithium-ion battery anode. *Energy. Fuels.* **2024**, *38*, 8306-16. DOI
- Yu, K.; Wang, Y.; Wang, X.; Liu, W.; Liang, J.; Liang, C. Preparation of porous carbon anode materials for lithium-ion battery from rice husk. *Mater. Lett.* **2019**, *253*, 405-8. DOI
- Yoshio, M.; Wang, H.; Fukuda, K.; Hara, Y.; Adachi, Y. Effect of carbon coating on electrochemical performance of treated natural

- graphite as lithium-ion battery anode material. *J. Electrochem. Soc.* **2000**, *147*, 1245. DOI
26. Ren, W.; Li, D.; Liu, H.; et al. Lithium storage performance of carbon nanotubes with different nitrogen contents as anodes in lithium ions batteries. *Electrochim. Acta.* **2013**, *105*, 75-82. DOI
 27. Sun, C.; Xu, X.; Gui, C.; et al. High-quality epitaxial N doped graphene on SiC with tunable interfacial interactions via electron/ion bridges for stable lithium-ion storage. *Nano-Micro. Lett.* **2023**, *15*, 202. DOI PubMed PMC
 28. Li, H.; Yu, H.; Zhang, X.; et al. Bowl-like 3C-SiC nanoshells encapsulated in hollow graphitic carbon spheres for high-rate lithium-ion batteries. *Chem. Mater.* **2016**, *28*, 1179-86. DOI
 29. Zhang, Y.; Wu, B.; Mu, G.; Ma, C.; Mu, D.; Wu, F. recent progress and perspectives on silicon anode: synthesis and prelithiation for LIBs energy storage. *J. Energy. Chem.* **2022**, *64*, 615-50. DOI